Evaluation of a dynamic-diagnostic modelling approach to generate highly resolved wind fields in the Alpine region

Heimo Truhetz, Andreas Gobiet, and Gottfried Kirchengast

Wegener Center for Climate and Global Change (WegCenter) and
Institute for Geophysics, Astrophysics and Meteorology (IGAM),
University of Graz, Austria

Author's address: Heimo Truhetz, Wegener Center for Climate and Global Change, University of Graz, Austria
Leechgasse 25, A-8010 Graz, Austria
Email: heimo.truhetz@uni-graz.at

Abstract

For generating highly resolved wind fields in the Alpine region the presented work focuses on the evaluation of a hybrid dynamic-diagnostic downscaling procedure. The diagnostic model CALMET is driven by the dynamic model MM5, which is nested into ECMWF's re-analysis ERA-40. Near surface winds are downscaled via multiple nesting from ~120 km to 200 m grid spacing without ingestion of any further observational data for the test period between 7 September to 15 November 1999 within a mountainous study area (140 km x 70 km) located in the eastern Alps (Hohe Tauern). Two MM5 grid spacings for driving the diagnostic model were evaluated, 5 km and 10 km, respectively. Detailed error statistics based on observations from surface stations show drastic improvements of modelled air-flows compared to the grossly deviating driving data (ERA-40). The overall bias relative to the station-averaged observed mean wind speed of 5.8 m/s is systematically reduced from –4.1 m/s to –0.7 m/s. In general, low wind speeds are slightly overestimated, while higher wind speeds are increasingly underestimated.
A reduction of the finest horizontal grid resolution of the dynamic model from 5 km to 10 km, which would be computationally favourable, induces additional errors with respect to unresolved air flows, which the diagnostic model is unable to correct in most cases. Important wind climatologic characteristics (e.g., bimodal frequency distributions) disappear, which accentuates the importance of high-quality, high-resolution initial wind fields for diagnostic models operating in complex terrains.

Zusammenfassung

Das Ziel der vorliegenden Arbeit ist die Evaluation eines kombinierten dynamisch-diagnostischen downscaling Verfahrens zur Erstellung hoch aufgelöster Windfelder im Alpenraum. Dazu wird das diagnostische Modell CALMET mit dem dynamischen Modell MM5 angetrieben, welches in den Re-Analysedatensatz ERA-40 des EZMW eingebettet wird. Bodennahe Luftströmungen werden ohne weitere Zuhilfenahme von Beobachtungsdaten im Testzeitraum vom 7. September bis zum 15. November 1999 für eine gebirgige Testregion (140 km x 70 km) im ostalpinen Raum (Hohe Tauern) von einer horizontalen Auflösung von ~120 km (ERA-40) durch mehrfaches Nesting auf 200 m gebracht. Zwei horizontale Gitterweiten der MM5-Antriebsfelder für das diagnostische Modell wurden getestet, 5 km und 10 km. Eine ausführliche Fehlerstatistik basierend auf Windmessdaten von Bodenstationen zeigt eine drastische Verbesserung der modellierten Luftströmungen im Vergleich zu den sehr stark abweichenden Antriebsdaten (ERA-40). Der Gesamtbias wird relativ zur gemessenen mittleren Windgeschwindigkeit von 5.8 m/s systematisch von –4.1 m/s auf –0.7 m/s reduziert. Generell tritt eine geringe Überschätzung niedriger Windgeschwindigkeiten auf, während höhere Windgeschwindigkeiten zunehmend unterschätzt werden.
Bei einer Reduktion der höchsten Horizontalauflösung des dynamischen Modells von 5 km auf 10 km, was hinsichtlich der Rechenzeit von Vorteil wäre, werden kleinräumige Luftströmungen nicht mehr erfasst, wodurch zusätzliche Abweichungen induziert werden, die das diagnostische Modell meist nicht mehr korrigieren kann. Wichtige windklimatologische Charakteristika (z.B. bimodale Häufigkeitsverteilungen) gehen dabei verloren, was den Bedarf diagnostischer Modelle an qualitativ hochwertigen und räumlich hoch aufgelösten Initialisierungsfeldern im komplexen Gelände unterstreicht.

1 Introduction

Early spatially distributed wind climatologies (e.g., TROEN and PETERSEN, 1989) based on the analysis of JACKSON and HUNT (1975) were trying to take into account variations of terrain heights and surface roughness lengths in a statistical manner. Satisfactory results were only achieved in homogenous and flat terrain (DOBESCH and KURY, 1997). In complex terrain, observational data from closely located stations have to be ingested: BERGE et al. (2006) were able to reduce the uncertainties of the annual wind speed from ~25% to less than 6% by reducing the distances between surface stations from 45 km to less than 3 km. Nevertheless, the statistical methods are excessively applied in actual studies (BARTHOLY and RADICS, 2005) deriving frequency distributions and distribution fits (e.g., Rayleigh and Weibull functions) with respect to wind speed and direction, even if only a sparse station network is available.

On the other hand, diagnostic models, also called *kinematic* or *mass-consistent* models (RATTO et al., 1994), based on Jackson and Hunt's analysis as well (e.g., MASON and KING, 1985; XU et al., 1994) or on the mass conservation law like the California Meteorological Model (CALMET) (SCIRE et al., 2000) are using simple divergence minimisation schemes (e.g., GODDIN et al, 1980), variational techniques (RATTO et al., 1994) with adaptive grids (MONTERO et al., 2005), or solve non-linear differential equations in spectral space (XU et al., 1994) to fulfil the constraints of mass-consistency for steady incompressible flow and apply additional correction algorithms like terrain induced flow perturbations, thermodynamic blocking effects, effects of variable surface roughness lengths, and effects of atmospheric stability. However, the quality of the initial first guess field is of vital importance. GROSS (1996) concludes that 50-100 observation sites per study area (~25 km x 25 km) should be used in hilly terrain. Evaluation studies for short term (~1 day) simulations report biases of mean wind speeds from –20% to 28% (500 m grid spacing) in the Alpine region (DESIATO et al.,1998). More specifically, Cox et al. (2005), who compared diagnostic models in less complex terrain (~1 km grid spacing) driven by observational data (distances between the stations ~5.8 km), found an underestimation of mean wind speeds in general (e.g., –11.0% bias for CALMET) and best performances during unstable conditions (correlation coefficients 0.5-0.6).

The most sophisticated modelling approaches (e.g., Large-Eddie-Simulations, LES) are implemented in up-to-date dynamic models like the PSU/NCAR model MM5 (DUDHIA et al., 1993), which are widely used in the fields of dynamic downscaling and regional climate modelling (e.g., YARNAL et al., 2001). They are able to simulate turbulent flow splitting, thermal effects, and effects due to changing pressure gradients and can be applied to any location regardless of the availability of local observational data by driving them with lateral boundary conditions derived from meteorological analyses like those of the European Centre of Medium-Range Weather Forecasts (ECMWF). A further general advantage of dynamic downscaling is the ability to create future scenarios by downscaling results of global climate models. The performance with respect to near surface winds is comparable with observation-based diagnostic models in some cases (RATTO et al., 1994), but simulations of long periods (i.e., decades) at high resolution (grid spacing < 10 km) are exceeding current computational resources.

To reduce the computational load, dynamic models have been applied to certain classes of weather patterns (dynamic-statistical downscaling) and generated wind climatologies with different accuracies depending on the model's resolutions and the complexity of the terrain: biases of the mean wind speeds of ~20% were found over the greater Alpine region and the eastern Adriatic coast (20 km grid spacing) (FUENTES and HEIMANN, 1996; HEIMANN, 2001) and MENGELKAMP (1999) achieved biases of about –4% in central Germany (1 km grid spacing). Two of the disadvantages of these methods are the reduced representation of the whole variety of weather phenomena by a limited number of classes and discontinuities in the model's soil fields, caused by class-specific model re-initialisations.

Other downscaling techniques like physical (ACHBERGER et al., 2002) or physical-statistical (DE ROOY and KOK, 2004) methods are deriving highly resolved near surface wind fields from larger-scale flows via Monin-Obukhov similarity theory. However, since MOARES et al. (2005) demonstrated the limited applicability of this theory in complex terrain, the physical methods are not supposed to add significant value in mountainous regions with steep slopes.

The approach described in this paper was designed to be independent from observational data, to avoid the shortcomings of the dynamic-statistical approaches, but still to be computationally feasible for long-term simulations (decades) in order to generate highly resolved wind climatologies as it is planned in our future work. We combined a dynamic (MM5) with a diagnostic model (CALMET) (dynamic-diagnostic

downscaling, see Section 2) as it has already been proposed in air-quality studies (BARNA and LAMB, 2000; CHANDRASEKAR et al., 2003). The focus lies on the evaluation of the performance of our downscaling approach in very complex terrain and on investigating the influence of MM5's horizontal grid spacing on the resultant wind fields by means of two testbed simulations over an inner Alpine region (Section 3). Conclusions are drawn in Section 4.

2 Methodology and simulation setup

2.1 Methodology

The hybrid dynamic-diagnostic downscaling procedure consists of two main steps:
First, global atmospheric analyses or atmospheric fields from global climate models (GCMs) are dynamically downscaled with MM5 (version 3.7.3) to derive atmospheric fields at mesoscale resolution. Following experiences in dynamic downscaling in complex terrain (ZÄNGL et al., 2004; LOIBL et al., 2006) an updated cumulus parameterisation with shallow convection (KAIN, 2004), the ETA boundary layer scheme (JANJIC, 1990; JANJIC 1994), a mixed-phase explicit moisture scheme (REISNER et al., 1998), the Rapid Radiative Transfer Model (RRTM) (MLAWER et al. 1997), and the NOAH land surface model (CHEN and DUDHIA, 2001) were selected. Although ZÄNGL et al. (2004) have shown that calculating MM5's horizontal diffusion in Cartesian coordinates leads to promising results, we considered it as computationally too costly (+25%) for our future objectives which include long-term simulations.
In a double re-gridding step, the mesoscale MM5 fields are interpolated onto CALMET's finer grid taking into account local terrain variability and the circumstance that MM5 and CALMET work in different geographic projections: The MM5 fields are firstly interpolated onto an intermediate grid with 1 km grid spacing using an overlapping parabolic method as implemented in the MM5 preprocessor NESTDOWN (MANNING and HAAGENSON, 1992). While the vertical wind components are neglected, the interpolated horizontal wind components are adjusted regarding to their new altitudes on the 1 km grid via vertical gradients linear in pressure. In addition, the divergence of the vertically averaged wind field is removed assuming that the correction terms can be derived from a two dimensional potential flow. Afterwards, these intermediate fields (1 km grid spacing) are interpolated to CALMET's grid using a simple inverse distance method in horizontal direction. Since the models are using different vertical terrain-following coordinates (sigma-pressure coordinate in MM5 and height above ground in CALMET), vertical interpolation is performed via a cubic-spline method.
The second main step is the application of a modified version of the diagnostic model CALMET. After initialisation of the horizontal wind field, CALMET induces vertical wind components (with an exponential decay in height above ground) regarding to terrain slope angles (LIU and YOCKE, 1980) and applies a two-dimensional divergence-minimisation scheme (GOODIN et al., 1980) to the horizontal wind components to fulfil the continuity equation. Furthermore, slope flows enforced by sensible heat fluxes and thermodynamic blocking effects depending on the temperature lapse rate from MM5 (spatially averaged over the study area) are induced generating additional divergence in turn. This divergence is removed by re-adjusting the vertical wind components in a final step.
Based on the local energy budget at the surface (HOLTSLAG and VAN ULDEN, 1983), latent, sensible, and soil (vanishing into the ground) heat fluxes are calculated from the Bowen-ratio (β), the ratio between the soil heat flux and net radiation (referred to as soil heat flux parameter, h_{fx}), which are externally given (see below), and from the net horizontal surface radiation. Following HOLTSLAG and VAN ULDEN (1983) the net radiation is derived from the solar radiation, the surface albedo and the cloud cover fraction (interpolated from MM5, see above) with respect to slope angles, but topographic shading is neglected.
In addition to the Bowen-ratio (β) and the soil heat flux parameter (h_{fx}) CALMET's parameterisations are requiring the surface roughness length (z_0), the snow-free surface albedo (α), and terrain heights separately for each grid cell. A more detailed description of CALMET can be found in GODFREY and CLARKSON (1998), SCIRE et al. (2000), and references therein.
The geo-physical parameters (z_0, α, β, and h_{fx}) were taken from literature (BMU, 2002; HAGEMANN, 2002; PINEDA et al., 2004; SCIRE et al., 2000) (see Table 1) and are statically linked to the highly resolved land cover information from the CORINE land cover data set CLC90 (EEA, 1995), version 12/2000, which are re-sampled to CALMET's grid via the nearest-neighbourhood method. Terrain heights were derived from NASA's Shuttle Radar Topography Mission (SRTM) (RABUS et al., 2003), where missing values were approximated via spline-interpolation techniques (MITASOVA and MITAS, 1993).
In contrast to the original CALMET code, where no snow cover effects are considered, a simple parameterisation of the effect of snow cover on surface

albedo is implemented in the following way: MM5's simulated snow heights are firstly interpolated onto the intermediate grid (1km grid spacing, see above) and secondly transferred to CALMET's grid via the nearest-neighbourhood method. Based on these snow heights on the CALMET grid ($h_{sh,MM5}$) and the snow-free albedo (α, Table 1), CALMET's surface albedo (α_{CALMET}) is calculated from (2.1):

$$\alpha_{CALMET} = \begin{cases} 1.5 \cdot \alpha, & \forall h_{sh,MM5} > 0.01\,\mathrm{m} \\ \alpha \end{cases} \quad (2.1)$$

Note that the transformation of snow heights from the coarse MM5 grid to the much higher resolved CALMET grid neglects any sub-grid scale effects beyond the MM5 grid.
Opposite to other mass-consistent models CALMET induces slope flows and thermodynamic blocking effects, which are promising features in very complex terrain. In addition, the simplicity of the divergence minimisation scheme keeps the amount of computational resources on a maintainable level, even if the number of grid points is very large (4.9×10^6 in our study area).
However, we found very high vertical wind components during model testing (similar to COX et al. (2005)) accompanied by unrealistic horizontal components. To overcome this difficulty the vertical components were damped right after initialisation by a factor of 0.3, since damping influences the horizontal components via the two-dimensional divergence minimisation scheme. The factor was empirically derived by comparing the horizontal wind speeds from numerous CALMET runs with observation data (not shown). Note that any damping factor unequal to 1.0 in principle violates the physical relations.
In addition to this model-deficiency, CALMET has several other shortcomings: flow-splitting effects, cross-valley circulations due to surface inversion-layers, and other dynamic effects are not included, the temporal resolution is limited to the temporal storage interval of the initialisation fields, and since MM5 data are limited to grid cell averages, turbulence induced increase of wind speeds and extreme events (wind gusts) are not expected to be found in CALMET's output.

2.2 Experimental setup

The downscaling method is applied to the Hohe Tauern region (study area: 140 km x 70 km, altitude from ~190 m to 3798 m, the Großglockner) in the Eastern Alps (Figure 1) to downscale near surface winds in the period from 7 September to 15 November 1999, where good observational data exist for validation from the Mesoscale Alpine Programme (MAP) (BOUGEAULT et al., 2001).
MM5 is driven by lateral boundary conditions derived from ECMWF's reanalysis ERA-40 (~ 120 km x 80 km grid spacing; UPPALA et al., 2004). Two different dynamic downscaling settings (referred to as case A and case B) are chosen. While in case A, ERA-40 is downscaled with MM5 in three nested domains (45 km, 15 km and 5 km grid spacing), in case B MM5 runs in two nests (30 km and 10 km grid spacing) (Figure 1a). The vertical discretisation is carried out in 42 levels for case A and 29 levels for case B; MM5's top level is placed at 100 hPa in both cases. A more detailed description of the MM5 setup is given in Truhetz et al. (2005). Hourly time-slices of the dataset of the finest resolved nest of each case are used to generate CALMET's initial wind fields in the study area (Figure 1c) with 200 m grid spacing which is the target resolution of this study. Vertically, CALMET uses 20 levels in terrain-following coordinates in both cases. Since CALMET's parameterisations are related to processes within the planetary boundary layer (PBL) the model's top is placed at 1250 m above ground level (a.g.l.) which includes 98.8% of all PBL heights simulated with MM5 in domain A3 (Figure 1a); the lowest level is fixed at 10 m (a.g.l.).

3 Results and discussion

Figure 2 depicts the wind fields for a small part of the study area (Figure 1c) 30 m a.g.l. at a certain time slice before (left panels) and after (right panels) the diagnostic downscaling step for case A (top panels) and B (bottom panels). CALMET turns wind vectors in valleys in a realistic way, while they are nearly left unchanged on mountain ridges and tops. Though this qualitative comparison leads to very similar results in case A and case B, we found considerable quantitative differences as will be demonstrated below.
To investigate the method's performance quantitatively, the downscaled wind fields were compared to observations (10 minutes mean values of wind speed and wind direction from selected surface stations) from the MAP period within 7 September to 15 November 1999 (see Figure 1c for the locations of the stations and Table 2 for general station information). Since CALMET's lowest model level is fixed at 10 m a.g.l., only stations with anemometer heights greater than or close to 10 m a.g.l. are taken into account in order to avoid vertical extrapolation errors. Additionally, stations located closer than the tenfold anemometer height to an edge of a land-use

category in real world and on the CALMET grid dropped out as well to minimise possible influences from internal boundary-layers. To reduce the influence of observation errors pairs of observed and modelled data are neglected when the observed wind speed is less than the anemometer's speed of response (0.5 m/s). One of the stations (SB) broke down as from 16 September to the end of the simulation period, reducing the number of valid data records.
For the evaluation, the modelled horizontal wind components were horizontally interpolated bi-linearly from the model grid to the location of the station for each model layer. Subsequently, the velocities were vertically interpolated to the anemometer heights by cubic spline interpolation (h > 10 m a.g.l.) or extrapolated using the logarithmic wind profile for stable conditions (h < 10 m a.g.l.); the directions were linearly inter- and extrapolated.
From the differences between modelled and observed wind speeds and directions (taking into account cyclicality) biases (V_{BIAS} [m/s], DIR_{BIAS} [°]) and standard deviations (V_{STDEV} [m/s], DIR_{STDEV} [°]) as well as the linear Pearson's correlation coefficients of velocity (r_V [1]), their significance levels (p_{rv} [1]) from Student's t-test, and the observed mean wind speeds (V_{MEAN} [m/s]) were calculated separately for each station for case A and case B. Additionally, the root mean square error for vectors (V_{RMS} [m/s]) (3.1),

$$V_{RMS} = \sqrt{\frac{\sum_{i=1}^{N}\left[\left(u_m^i - u_o^i\right)^2 + \left(v_m^i - v_o^i\right)^2\right]}{N}}, \qquad (3.1)$$

was computed to combine directional and wind speed errors.
An overview of the error statistics is given in Table 3. The general success of the method is demonstrated by the improvement of any error measure in both cases A and B (Tables 3b and 3d) compared to the driving data (ERA-40, Table 3e). Particularly, the correlation coefficients increase from virtually uncorrelated (below 0.1) to statistically significant 0.4–0.7 ($p_{rv} < 0.01$) in case A (except station SH, see discussion below). Note that ERA-40 has a storage interval of 6 hours and therefore the error statistics are based on a smaller sample size than for the downscaling results.
In case A, stations IF, PK, RH, and SB as well as the averages over all stations (weighted by the number of valid data) show a systematic error reduction from the dynamic (Table 3a) to the diagnostic (Table 3b) downscaling step: V_{RMS} is reduced by 11%, V_{BIAS} by 66%, V_{STDEV} by 3%, and DIR_{STDEV} by 11% (regarding large values of DIR_{STDEV}, small changes in DIR_{BIAS} are not relevant). r_V is increased by 9%. However, error characteristics at EB and SH are unchanged or slightly degraded.
EB is located at the eastern side-slope of a north-south oriented valley (the Wipp Valley), which aligns to the main wind direction of the characteristic weather phenomena for the study period (south-foehn). Thus EB is already well captured by the dynamic downscaling step and the diagnostic model is unable to further improve the result in that case.
SH is dominated by strong easterly local thermal winds (not shown), which are virtually uncorrelated to the large scale flow and could not be resolved by the dynamic model (Table 3a). This provides misleading initialisation fields to the diagnostic model and induces additional random errors ($V_{RMS} > V_{MEAN}$, V_{STDEV}, DIR_{STDEV}, Table 3b).
Even though the diagnostic model improves the error statistics at IF, air flows are poorly simulated in general, because IF is strongly influenced by a steep mountain chain (the Nordkette) enforcing easterly and westerly flows. These main directions are captured by the model partly in an asynchronous manner (not shown), resulting in large directional errors (DIR_{STDEV}, Table 3b).
In case B V_{BIAS} is decreased (by 66%), the other error statistics are nearly left unchanged (V_{RMS}, Table 3d) or get worse (V_{STDEV}, DIR_{STDEV}, r_V in Table 3d). This behaviour is reflected separately for each station, except for EB, where the results are comparable to those in case A. The reason is that the 10 km grid spacing of the dynamical model in case B fails to provide sufficiently resolved initialisations fields for the high resolution diagnostic model, leaving it unable to further correct flow field deficiencies.

More information about the method's performance can be derived from the wind velocity-dependent error distributions (Figures 3 and 4).
Slow wind speeds (< 5 m/s) are somewhat overestimated while velocities above 5 m/s are increasingly underestimated (Figure 3). Since MM5's results show the same behaviour in both cases (Figure 3a and 3c) the increase of the resolution is too small to resolve the turbulence induced increase of wind speeds. Simultaneously, directions are more accurately captured at higher wind speed (Figure 4).
Note that the classification of the observed wind speeds into low (< 5 m/s), medium (5-15 m/s), and high (≥ 15 m/s) affects the medians of each class shown in Figure 3 and 4. Since the errors of speed change their signs in the first class (Figure 3), low medians of this class do not directly correlate with small errors.

As already shown in the general error statistics (Table 3), the velocity-resolved statistics of any downscaling-case (Figures 3a-3d and 4a-4d) show huge improvements compared to the driving data (Figures 3e and 4e).
Looking into details, case A demonstrates the importance of the diagnostic downscaling step (Figures 3b and 4b): compared to the dynamic downscaling step (Figures 3a and 4a) the underestimation of wind speed is decreased by 40% for medium and by 44% for high wind speeds. The statistical spreads of the directional errors expressed as the differences between the absolute arithmetic means of the quartile-ranges (25%-75% quantile) of each class are successively reduced from 147° to 117° (class low), 60° to 52° (class medium), and 43° to 28° (class high), while the medians are small in both cases.
In case B, the diagnostic step yields a smaller reduction of the underestimation of speed (36% for medium and 15% for high wind speeds, Figures 3c, 3d). Although the directional errors are reduced (32% for medium and 93% for high wind speeds) they are featuring large positive biases for medium wind speeds even after the diagnostic step and increasing spreads of the class-wide quartile-ranges (55° to 57°, 42° to 57° for medium and high wind speeds, respectively; Figures 4c, 4d).
A climatological analysis of observed air flows revealed bimodal frequency distributions for wind speed and direction at all stations except IF and SH. As an example, the frequency distributions of modelled and observed air flows for the station EB are shown in Figure 5. In case A (Figure 5a) the observed (Figure 5c) bimodal characteristic of the frequency distribution of wind speed (limiting the usability of the fitted unimodal Rayleigh and Weibull distribution functions) is reproduced. In contrast, case B (Figure 5b) displays an unimodal distribution. Since moderate and high wind speeds are generally underestimated, the distribution in case A is condensed towards lower wind speeds. The positive bias (Table 3b) is a result of the overestimation of the more frequent low speeds. Also the observed bimodal directions and the mean and maximum wind speed of each directional class (caused by weak local katabatic winds and strong larger-scale winds (south-foehn)), are better represented in case A than in case B. Particularly the main wind direction with high velocities from south-east is well captured. The weak north-westerly components are clockwise twisted by ~ 80°.

4 Conclusions

The presented dynamic-diagnostic method successfully downscales near surface winds from the meso-alpha (grid spacing ~120 km) to the microscale (grid spacing 200 m) by multiple nesting of a dynamic model (MM5) into the ERA-40 re-analysis and a subsequent diagnostic downscaling step (CALMET). The results show a reasonably realistic behaviour over complex terrain and strongly improved error statistics compared to the driving data. In general, exposed sites and sites dominated by large-scale flows are better captured since the general flow is already sufficiently well simulated by the finest resolved dynamic downscaling step. However, the diagnostic downscaling step is particularly effective at less exposed sites, where the dynamic model shows large errors.
Generally, low wind speeds are somewhat overestimated and show large directional uncertainties, while medium and high wind speeds are increasingly underestimated because of the stationarity assumption of CALMET and the coarse grid spacing of MM5. Directional errors are drastically reduced at higher wind speeds.
The quality of the initial wind fields of the diagnostic model (from MM5) is of vital importance for the resultant wind fields. While CALMET is able to add value to 5 km MM5 fields, a resolution reduction of MM5 to 10 km grid spacing induces errors with respect to unresolved air flows, which the diagnostic model is unable to correct in most cases. Reducing the grid spacing ratio between the dynamic and diagnostic downscaling step from 50 (case B) to 25 (case A) is an indisputable necessity for the generation of wind fields and climatologies in the given terrain. Moreover, the observed bimodality of frequency distributions of wind speed (challenging many statistical downscaling approaches based on unimodal distribution functions) could only be reproduced using 5 km MM5 fields.
Promising further advancements of the presented downscaling method are related to the improved generation of initial wind fields for the diagnostic downscaling step, particularly by further increasing the resolution of the dynamical model to 1-3 km, following the practice of dynamical downscaling, where grid spacing ratios of about 10 or less are used in general. Further improvements of the initial wind fields are expected from more sophisticated grid interpolation techniques taking into account potential flow assumptions and wind directions.
Moreover, the calculation of CALMET's vertical wind components obviously needs to be reconsidered and further advances can be expected from the extension of the divergence minimisation scheme to fully three-dimensional potential flows, transition from averaged

to spatially resolved temperature gradients, inclusion of topographic shading effects and snow height downscaling methods, and the re-consideration and introduction of varying geo-physical parameters based on annual cycles. Also, an addition of a wind-gust estimation scheme is planned, which adds new capability for regional estimation of storm activities.

Acknowledgments

The work was partially funded by Austrian Research Centers systems research GmbH via the project "Research for Climate Protection: Model Run Evaluation (reclip:more)". Partial funding was also received from WegCenter's startup support for its Regional and Local Climate Modeling and Analysis Research Group (ReLoClim). Observational data were provided by the Austrian Central Institute for Meteorology and Geodynamics (ZAMG) and the Institute for Meteorology and Geophysics, University of Innsbruck, Austria.

Tables and Figures

Table 1: Most frequently used CORINE land-use categories (level 3) of the study area associated to surface roughness (z_0), snow-free surface albedo (α), Bowen-ratio (β), and soil heat flux parameter (h_{fx}). The categories' fraction of occurrence (*fract.*) is related to the grid of the diagnostic model (200 m grid spacing). The values are given in their precisions found in literature. (A full set of parameters is available from the author; all other categories exhibit fractions < 2.5%).

CORINE category (level 3)	z_0 **[m]**	α **[1]**	β **[1]**	h_{fx} **[1]**	***fract.*** **[%]**
coniferous forest	1.00	0.142	1.0	0.15	30.1
natural grassland	0.02	0.175	1.0	0.15	25.6
bare rock	0.20	0.181	1.0	0.15	14.0
pastures	0.02	0.166	1.0	0.15	9.6
sparsely vegetated areas	0.02	0.204	1.0	0.15	9.5
glaciers and perpetual snow	0.05	0.464	0.5	0.15	3.8

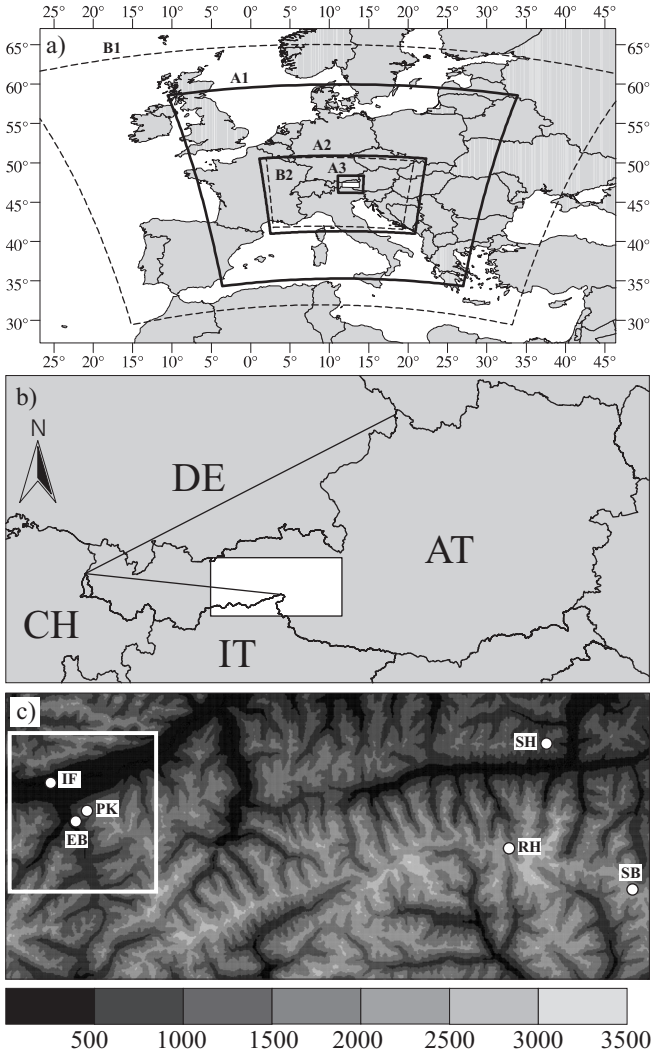

Figure 1: (a) Domain settings. Case A (solid lines): ERA-40 is dynamically downscaled to 45 km (A1), 15 km (A2), and 5 km (A3), and diagnostically to 200 m grid spacing in the study area (white). Case B (dashed lines): ERA-40 is dynamically downscaled to 30 km (B1), 10 km (B2), and diagnostically to 200 m grid spacing (white). (b) Location of the study area (white, Hohe Tauern region) in Austria. (c) Orography of the study area (140 km × 70 km) at 200 m grid spacing (grey scaled terrain heights [m]), observation sites (white marks), and an area shown in Figure 2 (white rectangle).

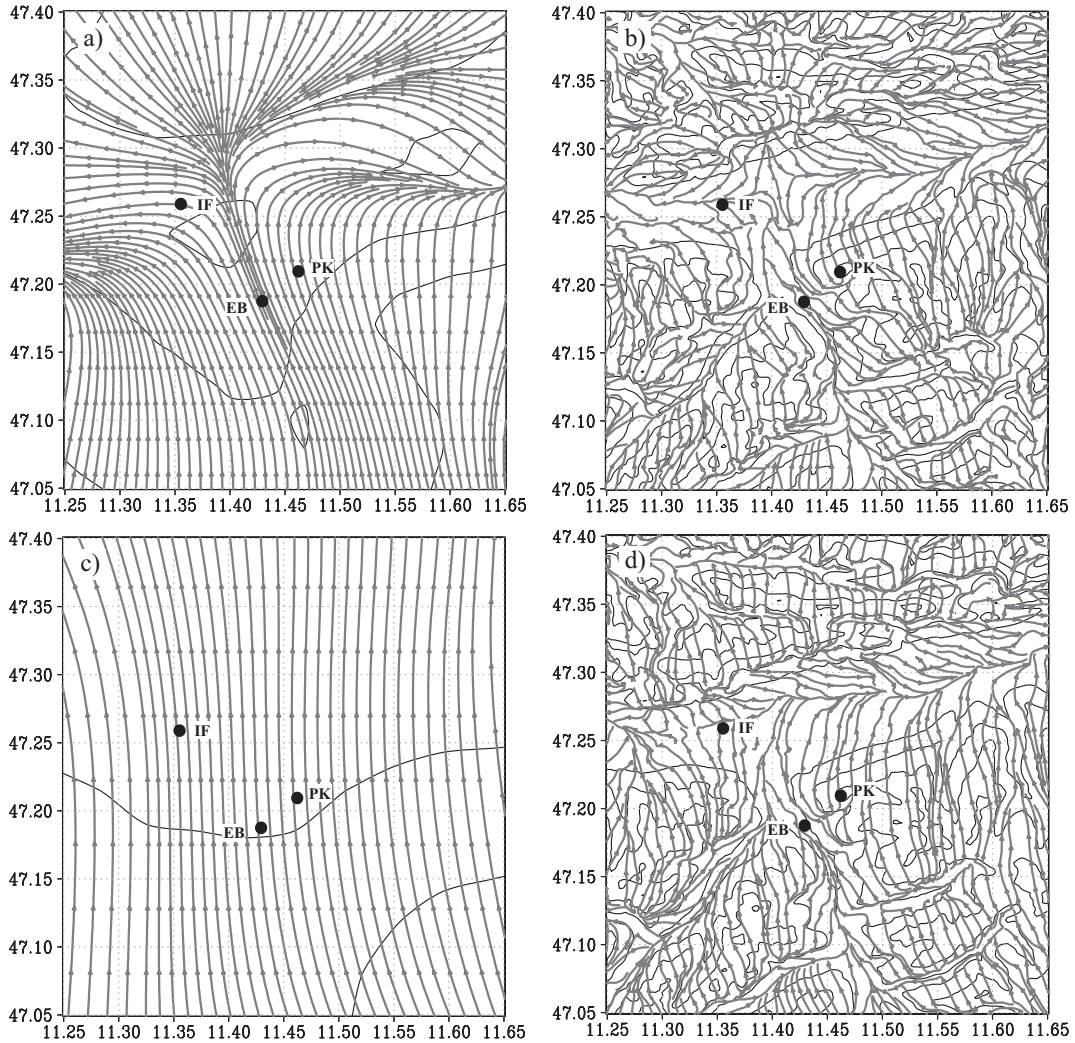

Figure 2: Modelled wind field 30 m a.g.l. (stream lines; 21 Oct. 1999 00:00 UTC; Wipp Valley). MM5 data with 5 km grid spacing (a) is downscaled to 200 m grid spacing (b) (case A), and MM5 data with 10 km grid spacing (c) is downscaled to 200 m grid spacing (d) (case B). The sites of the stations "Innsbruck-Flugplatz" (IF), "Ellboegen" (EB), and "Patscherkofel" (PK) are marked.

Table 2: General information on observation stations: latitude (φ), longitude (λ), altitude (*alt.*), anemometer height a.g.l. (h), number of data values (N), and World Meteorological Organisation (WMO) identification number.

name of station	φ [°]	λ [°]	***alt.*** **[m]**	***h*** **[m]**	***N***	**WMO**
Innsbruck-Flugplatz (IF)	47.2589	11.3553	579	32	1066	11120
Patscherkofel (PK)	47.2094	11.4622	2247	7	1166	11126
Rudolfshuette (RH)	47.1339	12.6256	2304	10	1365	11138
Sonnblick (SB)	47.0544	12.9578	3105	16	298	11146
Schmittenhoehe (SH)	47.3297	12.7367	1973	12	1475	11340
Ellboegen (EB)	47.1875	11.4294	1080	10	1291	77268

Table 3: Statistics of the differences between modelled and observed wind fields at observation stations of the finest dynamic and the diagnostic downscaling step of case A (a, b), and case B (c, d), and for the driving ERA-40 data (e). Observed mean wind speed (V_{MEAN}), root mean square error for vectors (V_{RMS}), biases and standard deviations for speed (V_{BIAS}, V_{STDEV}) and direction (DIR_{BIAS}, DIR_{STDEV}), linear correlation coefficient of wind speed (r_V), and its significant level (p_{rv}) over the period from 7 Sep. to 15 Nov. 1999 are given.

a) MM5 5 km (case A)	V_{MEAN} [m/s]	V_{RMS} [m/s]	V_{BIAS} [m/s]	V_{STDEV} [m/s]	DIR_{BIAS} [°]	DIR_{STDEV} [°]	r_V [1]	p_{rv} [1]
Innsbruck-Flugplatz (IF)	2.3	4.8	1.0	2.0	-1.0	115.2	0.37	< 0.01
Patscherkofel (PK)	8.8	9.5	-5.8	6.4	-22.8	85.3	0.59	< 0.01
Rudolfshuette (RH)	7.0	7.3	-1.4	6.1	-4.8	67.9	0.29	< 0.01
Sonnblick (SB)	11.6	9.3	-5.6	5.7	-4.9	55.1	0.66	< 0.01
Schmittenhoehe (SH)	4.6	5.2	-2.6	2.8	-0.7	96.9	0.19	< 0.01
Ellboegen (EB)	5.0	4.1	-0.5	2.8	13.6	67.8	0.73	< 0.01
6 station average	5.8	6.3	-2.1	4.1	-2.9	84.3	0.44	< 0.01
b) CALMET 200 m (case A)	V_{MEAN} [m/s]	V_{RMS} [m/s]	V_{BIAS} [m/s]	V_{STDEV} [m/s]	DIR_{BIAS} [°]	DIR_{STDEV} [°]	r_V [1]	p_{rv} [1]
Innsbruck-Flugplatz (IF)	2.3	3.7	-0.4	1.8	-38.0	101.4	0.40	< 0.01
Patscherkofel (PK)	8.8	6.8	-1.1	5.9	-15.4	63.6	0.63	< 0.01
Rudolfshuette (RH)	7.0	7.0	-0.9	5.5	-8.6	69.3	0.50	< 0.01
Sonnblick (SB)	11.6	8.5	-0.3	5.5	-0.7	53.6	0.70	< 0.01
Schmittenhoehe (SH)	4.6	5.2	-1.6	3.1	-0.5	85.4	0.16	< 0.01
Ellboegen (EB)	5.0	4.3	0.6	3.1	11.3	62.7	0.69	< 0.01
6 station average	5.8	5.6	-0.7	4.0	-8.5	75.0	0.48	< 0.01
c) MM5 10 km (case B)	V_{MEAN} [m/s]	V_{RMS} [m/s]	V_{BIAS} [m/s]	V_{STDEV} [m/s]	DIR_{BIAS} [°]	DIR_{STDEV} [°]	r_V [1]	p_{rv} [1]
Innsbruck-Flugplatz (IF)	2.3	5.0	1.7	2.4	-30.1	84.9	0.46	< 0.01
Patscherkofel (PK)	8.8	8.3	-5.0	5.7	15.4	68.8	0.78	< 0.01
Rudolfshuette (RH)	7.0	6.5	-2.2	5.1	-5.4	64.0	0.56	< 0.01
Sonnblick (SB)	11.6	10.6	-5.7	5.6	-13.7	58.4	0.68	< 0.01
Schmittenhoehe (SH)	4.6	4.8	-1.5	2.9	27.0	68.4	0.21	< 0.01
Ellboegen (EB)	5.0	6.0	-0.9	3.0	34.3	64.6	0.70	< 0.01
6 station average	5.8	6.3	-1.8	3.9	8.8	69.0	0.54	< 0.01
d) CALMET 200 m (case B)	V_{MEAN} [m/s]	V_{RMS} [m/s]	V_{BIAS} [m/s]	V_{STDEV} [m/s]	DIR_{BIAS} [°]	DIR_{STDEV} [°]	r_V [1]	p_{rv} [1]
Innsbruck-Flugplatz (IF)	2.3	3.0	-0.5	2.0	-1.4	80.3	0.20	< 0.01
Patscherkofel (PK)	8.8	7.8	-2.3	5.3	7.0	68.3	0.70	< 0.01
Rudolfshuette (RH)	7.0	7.8	-0.9	5.9	-8.9	77.6	0.33	< 0.01
Sonnblick (SB)	11.6	10.9	-3.2	6.4	-9.9	59.4	0.51	< 0.01
Schmittenhoehe (SH)	4.6	6.5	1.6	3.7	24.8	67.2	0.17	< 0.01
Ellboegen (EB)	5.0	4.9	-0.7	3.0	17.4	65.4	0.69	< 0.01
6 station average	5.8	6.3	-0.6	4.2	7.6	70.9	0.42	< 0.01
e) ERA-40 T106	V_{MEAN} [m/s]	V_{RMS} [m/s]	V_{BIAS} [m/s]	V_{STDEV} [m/s]	DIR_{BIAS} [°]	DIR_{STDEV} [°]	r_V [1]	p_{rv} [1]
Innsbruck-Flugplatz (IF)	2.3	5.6	2.4	3.5	27.7	87.7	0.11	0.08
Patscherkofel (PK)	8.8	12.2	-5.0	7.8	-21.9	101.0	-0.04	0.72
Rudolfshuette (RH)	6.9	10.4	-4.8	6.0	-57.2	100.5	0.15	0.01
Sonnblick (SB)	11.7	14.1	-11.1	7.4	-0.9	135.4	-0.04	0.70
Schmittenhoehe (SH)	4.6	5.9	-3.5	2.8	-3.6	122.8	0.10	0.06
Ellboegen (EB)	5.1	6.4	-3.6	4.1	1.5	91.0	0.06	0.19
6 station average	6.4	8.8	-4.1	5.1	-10.8	106.0	0.06	0.26

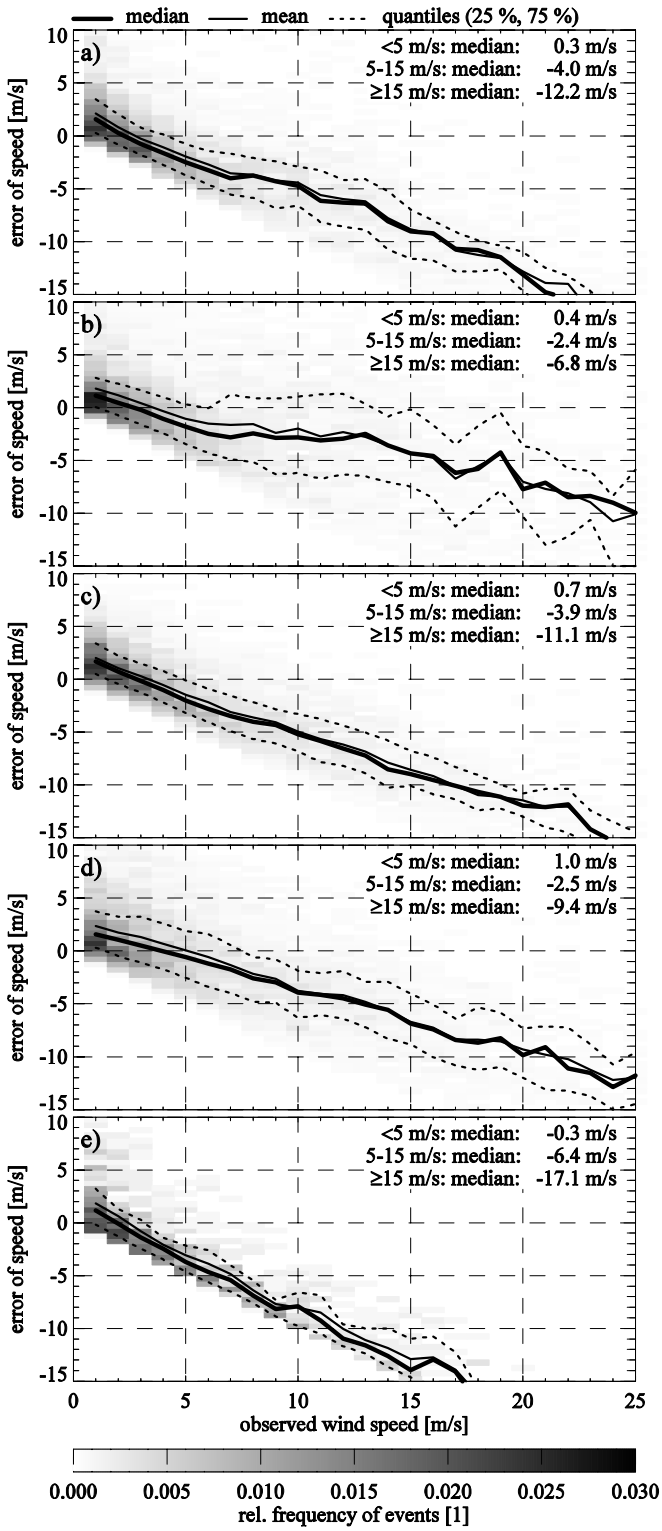

Figure 3: Differences between modelled and observed wind speeds. Case A: MM5 data with 5 km grid spacing (a) is downscaled to 200 m (b). Case B: MM5 data with 10 km grid spacing (c) is downscaled to 200 m (d). Panel (e): Error statistics of the common driving data (ERA-40).

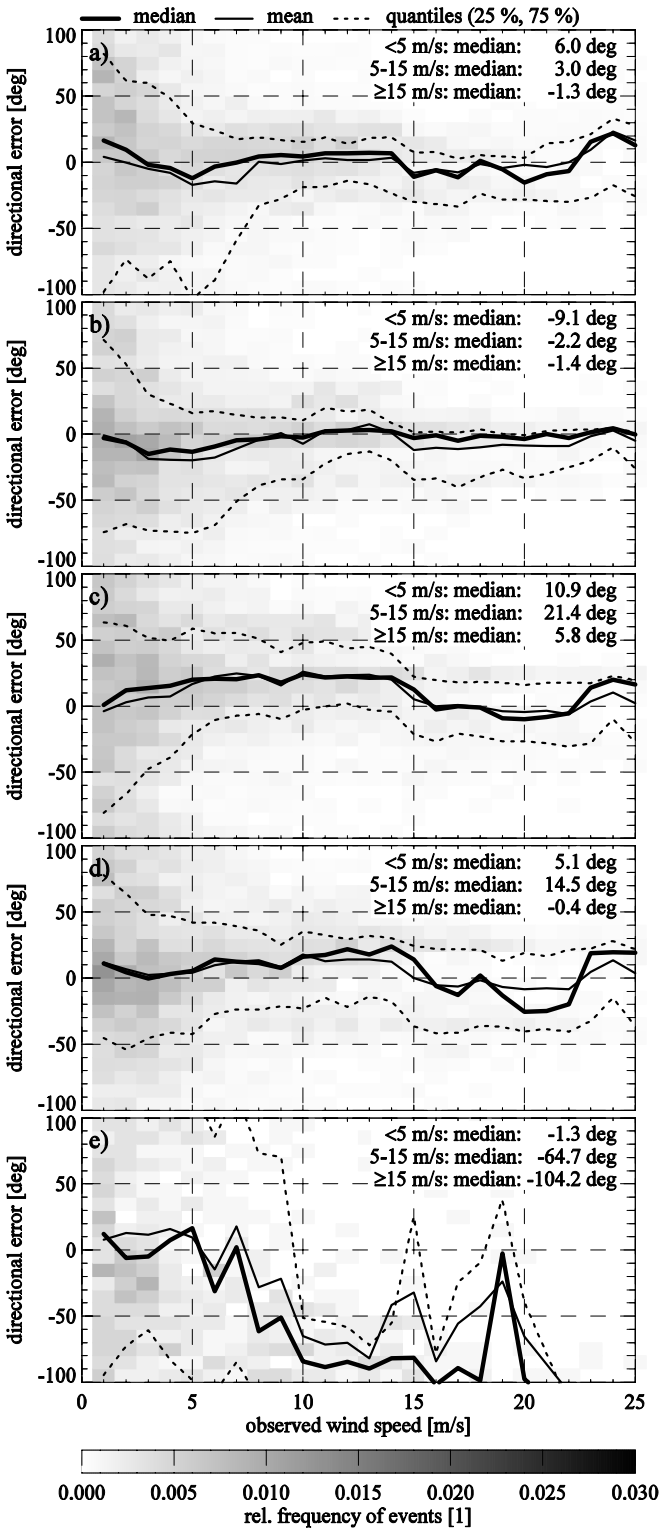

Figure 4: Differences between modelled and observed wind directions. Like Figure 3, but for wind directions.

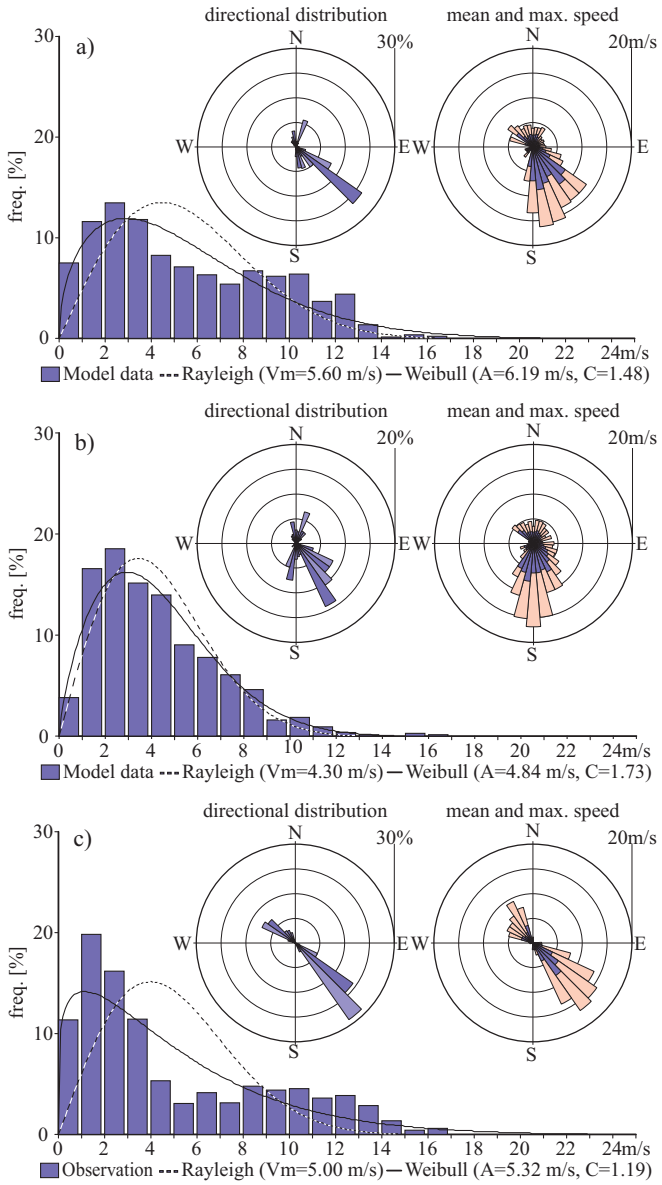

Figure 5: Frequency distributions of wind speed and direction of modelled data (200 m grid spacing) from case A (a), case B (b), and the observed data (c) at the station EB. Fitted Rayleigh- (dashed curves) and Weibull- (solid curves) functions are depicted.

References

ACHBERGER, C., M. EKSTRÖM, L. BÄRRING, 2002: Estimation of local near-surface wind conditions – A comparison of WAsP and regression based techniques. – Meteorol. Appl. **9**, 211-221.

BARNA, M., B. LAMB, 2000: Improving ozone modelling in regions of complex terrain using observational nudging in a prognostic meteorological model. – Atm. Env. **34**, 4889-4906.

BARTHOLY, J., K. RADICS, 2005: Wind profile and atmospheric stability over a complex terrain in southwestern part of Hungary. – Phys. Chem. Earth **30**, 195-200.

BERGE, E., F. NYHAMMER, L. TALLHAUG, 2006: An evaluation of the WAsP model at a coastal mountainous Site in Norway. – Wind Energy **9**, 131-140, DOI:10.10002/we191.

BMU, 2002: Erste Allgemeine Verwaltungsvorschrift zum Bundes-Immissionsschutzgesetz (Technische Anleitung zur Reinhaltung der Luft – TA Luft). – Bundesministerium f. Umwelt, Naturschutz und Reaktorsicherheit (BMU), Germany, Gemeinsames Minsterialblatt (GMBl.) **25-29**, 511-605.

BOUGEAULT, P., P. BINDER, A. BUZZI, R. DIRKS, R. HOUZE, J. KUETTNER, R. B. SMITH, R. STEINACKER, H. VOLKERT, 2001: The MAP Special Observing Period. – B. Am. Meteorol. Soc. **82**, 433-462.

CHANDRASEKAR, A., C.R. PHILBRICK, R. CLARK, B. DODDRIDGE, P. GEORGOPOULOS, 2003: Evaluating the performance of a computationally efficient MM5/CALMET system for developing wind field inputs to air quality models. – Atm. Env. **37**, 3267-3276.

CHEN, F., J. DUDHIA, 2001: Coupling an advanced land-surface/hydrology model with the Penn State/NCAR MM5 modelling system. Part I: Model implementation and sensitivity. – Mon. Wea. Rev. **129**, 569-585.

COX, R.M., J. SONTOWSKY, C.M. DOUGHERTY, 2005: An evaluation of three diagnostic wind models (CALMET, MCSCIPUF, and SWIFT) with wind data from the Dipole Pride 26 field experiments. – Meteorol. Appl. **12**, 329-341, DOI:10.1017/S1350482705001908.

DE ROOY, W.C., K. KOK, 2004: A combined physical-statistical approach for the downscaling of model wind speed. – Weather Forecast. **19**, 485-495.

DESIATO, F., S. FINARDI, G. BRUSASCA, M.G. MORSELLI, 1998: TRANSALP 1989 Experimental campaign – I. Simulation of 3D Flow with diagnostic wind field models. – Atm. Env. **32**, 1141-1156.

DOBESCH, H., G. KURY, 1997: Wind Atlas for the Central European Countries – Austria, Croatia, Czech Republic, Hungary, Slovak Republic and Slovenia. - Österreichische Beiträge zu Meteorologie und Geophysik **16**, 105pp.

DUDHIA, J., 1993: A nonhydrostatic version of the Penn State – NCAR mesoscale model: Validation and simulation of an atlantic cyclone and cold front. – Mon. Wea. Rev. **121**, 1493-1513.

EUROPEAN ENVIRONMENT AGENCY (EEA), 1995: CORINE Land Cover, European Environment Agency Report, Commission of the European Communities OPOCE (Office for official publications of the European Communities), Luxembourg.

FUENTES, U., D. HEIMANN, 1996: Verification of statistical-dynamical downscaling in the Alpine region. – Clim. Res. **7**, 151-168.

GOODIN, W.R., G.J. MCRAE, J.H. SEINFELD, 1980: An objective analysis technique for constructing three-dimensional urban-scale wind fields. – J. Appl. Meteorol. **19**, 98-108.

GODFREY, J.J., T.S. CLARKSON, 1998: Air quality modelling in a stable polar environment – Ross Island, Antarctica. – Atm. Env. **32**, 2899-2911.

GROSS, G., 1996: On the applicability of numerical mass-consistent wind field models. – Boundary-Layer Meterol. **77**, 379-394.

HAGEMANN, S., 2002: An improved land surface parameter dataset for global and regional climate models. – MPI Report **336**, Max Planck Institute for Meteorology, Hamburg.

HEIMANN, D., 2001: A model-based wind climatology of the eastern Adriatic coast. – Meteorol. Z. **10**, 5-16.

HOLTSLAG, A.A.M., A.P. VAN ULDEN, 1983: A simple scheme for daytime estimates of the surface fluxes from routine weather data. – J.Clim. and Appl. Meteor. **22**, 517-529.

JACKSON, P.S., J.C.R. HUNT, 1975: Turbulent flow over a low hill. – Quart. J. Roy. Meteor. Soc. **101**, 929-955.

JANJIC, Z.I., 1990: The step-mountain coordinate: Physical package. Mon. Wea. Rev. **118**, 1429-1443.

JANJIC, Z.I., 1994: The step-mountain eta coordinate model: Further development of the convection, viscous sublayer, and turbulent closure schemes. – Mon. Wea. Rev. **122**, 927-945.

KAIN, J. S., 2004: The Kain-Fritsch convective parameterization: An update. – J. Appl. Meteor. **43**, 170-181.

LIU, M.K., M.A. YOCKE, 1980: Siting of wind turbine generators in complex terrain. – J. Energy 4, 10-16.

LOIBL, W., A. BECK, M. DORNINGER, H. FORMAYER, A. GOBIET, W. SCHÖNER (Eds.), 2006: Kwiss-Programm reclip:more – research for climate protection: model run evaluation, Project year 2 – Report 2005, ARC systems research GmBH, Vienna, Austria.

MANNING, K.W., P.L. HAAGENSON, 1992: Data ingest and objective analysis for the PSU/NCAR mesoscale modeling system: Programs DATAGRID and RAWINS. – NCAR Technical Note TN-376+IA, National Center for Atmospheric Research, Boulder.

MASON, P.J., J.C. KING, 1985: Measurements and predictions of flow and turbulence over an isolated hill of moderate slope. – Quart. J. Roy. Meteorol. Soc. **111**, 617-640.

MENGELKAMP, H.T., 1999: Wind climate simulation over complex terrain and wind turbine energy output estimation. – Theor. Appl. Climatol. **63**, 192-139.

MITASOVA, H., L. MITAS, 1993: Interpolation by regularized spline with tension: I. Theory and implementation. – Mathematical Geology **25**, 641-655.

MLAWER, E. J., S. J. TAUBMAN, P. D. BROWN, M. J. IACONO, S. A. CLOUGH, 1997: Radiative transfer for inhomogeneous

atmosphere: RRTM, a validated correlated-k model for the longwave. – J. Geophys. Res. **102**, 16663-16682.
MONTERO, G., E. RODRÍGUEZ, R. MONTENEGR, J.M. ESCOBAR, J.M. GONZÁLEZ-YUSTE, 2005: Genetic algorithms for an improved parameter estimation with local refinement of tetrahedral meshes in a wind model. – Adv. Eng. Softw. **36**, 3-10.
MORAES, O.L.L., O.C. ACEVEDO, G.A. DEGRAZIA, D. ANFOSSI, R. DA SILVA, V. ANABOR, 2005: Surface layer turbulence parameters over a complex terrain. – Atm. Env. **39**, 3103-3112.
PINEDA, N., O. JORBA, J. JORGE, J.M. BALDASANO, 2004: Using NOAA AVHRR and SPOT VGT data to estimate surface parameters: application to a mesocale meteorological model. – Int. J. Remote Sens. **25**, 129-143.
RABUS, B., M. EINEDER, A. ROTH, R. BAMLER, 2003: The shuttle radar topography mission - a new class of digital elevation models acquired by spaceborne radar. – ISPRS J. Photogramm. **57**, 241-262.
RATTO, C.F., R. FESTA, C. ROMEO, 1994: Mass-consistent models for wind fields over complex terrain – the state-of-the-art. – Environmental Software **9**, 247-268.
REISNER, J., R. J. RASMUSSEN, R. T. BRUINTJES, 1998: Explicit forecasting of supercooled liquid water in winter storms using the MM5 mesoscale model. – Quart. J. Roy. Meteor. Soc. **124B**, 1071-1107.
SCIRE, J.S., F.R. ROBE, M.E. FERNAU, R.J. YAMERTINO, 2000: A User's Guide for the CALMET Meteorological Model (Version 5). – Earth Tech Inc., Concorde, http://www.src.com/verio/download/download.htm.
TROEN, I., E.L. PETERSEN, 1989: European Wind Atlas. Commission of the European Community, Risoe Nat. Lab., Roskilde.
TRUHETZ, H., A. GOBIET, G. KIRCHENGAST, 2005: Dynamical downscaling with MM5, upper air evaluation, and wind downscaling, reclip:more – WegCenter project report, Wegener Center, University of Graz, Austria.
UPPALA, S., P. KÅLLESBERG, A. HERNANDEZ, S. SAARINEN, M. FIORINO, X. LI, K. ONOGI, U. ANDREA, V. DA COSTA BECHTOLD, 2004: ERA-40: ECMWF 45-years reanalysis of the global atmosphere and surface conditions 1957–2002. – ECMWF News-letter **101**, 2-21.
XU, D., K.W. AYOTTE, P.A. TAYLOR, 1994: Development of a mixed spectral finite-difference model for turbulent boundary-layer flow over topography. – Boundary-Layer Meterol. **70**, 341-367.
YARNAL, B., A.C. COMRIE, B. FRAKES, D.P. BROWN, 2001: Developments and prospects in synoptic climatology. – Int. J. Climatol. **21**, 1923-1950, DOI:10.1002/joc.675.
ZÄNGL, G., A. GOHM, G. GEIER, 2004: South foehn in the Wipp Vally - Innsbruck region: Numerical simulations of the 24 October 1999 case (MAP-IOP 10). – Met. Atm. Phys. **86**, 213-243, DOI:10.1007/s00703-003-0029-8.